Article

Optimization of DC Energy Storage in Tokamak Poloidal Coils

Alessandro Lampasi [1,2,*] , Riccardo Testa [3,4], Bhavana Gudala [3,4] , Cristina Terlizzi [5] , Sabino Pipolo [1,2]
and Sandro Tenconi [3]

[1] Energy and Sustainable Economic Development (ENEA), Italian National Agency for New Technologies,
00044 Frascati, Italy; sabino.pipolo@enea.it

[2] DTT S. c. a r. l., 00044 Frascati, Italy

[3] OCEM Power Electronics, 40056 Valsamoggia, Italy; riccardo.testa@ocem.eu or riccardo.testa3@unibo.it (R.T.);
bhavana.gudala@ocem.eu or bhavana.gudala2@unibo.it (B.G.); sandro.tenconi@ocem.eu (S.T.)

[4] Department of Electrical, Electronic, and Information Engineering "Guglielmo Marconi", University of
Bologna, 40126 Bologna, Italy

[5] Department of Industrial Engineering, University of Rome Tor Vergata, 00133 Rome, Italy;
cristina.terlizzi@uniroma2.it

* Correspondence: alessandro.lampasi@enea.it

Abstract: Tokamaks are a very promising option to exploit nuclear fusion as a programmable and
safe energy source. A very critical issue for the practical use of tokamaks consists of the power flow
required to initiate and sustain the fusion process, in particular in the poloidal field coils. This flow
can be managed by introducing a DC energy storage based on supercapacitors. Because such storage
may be the most expensive and largest part of the poloidal power supply system, an excessive size
would cancel its potential advantages. This paper presents innovative strategies to optimize the DC
storage in poloidal power supply systems. The proposed solution involves the sharing of the DC
storage between different coil circuits. The study is supported by novel analytical formulas and by a
circuital model developed for this application. The obtained results show that this method and the
related algorithms can noticeably reduce the overall size of the storage and the power exchange with
the grid, providing a practical contribution toward the feasibility and the effectiveness of nuclear
fusion systems.

Keywords: nuclear fusion; tokamak; poloidal coils; DC storage; supercapacitors; power supply
systems; Divertor Tokamak Test (DTT)

1. Introduction

Control of nuclear fusion reactions is considered one of the most promising options
to generate programmable, clean, and safe energy on a large scale, as confirmed by the
growing investments by public institutions [1,2] and private companies [3]. Tokamaks use
high magnetic fields, produced by flowing a controlled current through coils, to confine
an extremely hot plasma where fusion reactions can occur [4]. The coils are oriented and
independently supplied according to the main component of the magnetic field they can
control. In the tokamak reference coordinates, these components are classified as toroidal
(TF) or poloidal (PF) fields, respectively [4]. As an evident trend, the TF and PF coils of
present and proposed tokamaks are made of superconducting materials operating at higher
and higher currents [5,6].

A very critical issue for the practical use of tokamaks as energy sources consists of the
optimization of the powers and energies necessary in the coils to initiate and maintain the
desired plasma configurations [7]. While in a tokamak the TF is practically constant, the
PF must change following a predefined scenario. This implies a variable flow of power
between each coil and its power supply (PS). In traditional systems, the PS is implemented
by AC/DC converters based on thyristor rectifiers that introduce a relevant contribution of
reactive power in the external grids [7,8]. The unavoidable consequence is that the tokamak

PF coils can demand powers on the order of 1 GVA from the grid [9]. Even though the total energy produced at the tokamak output could compensate for these demands [10,11], the technical and economic effectiveness of the process is difficult to sustain. Moreover, the huge and variable power flow at the interconnection nodes may be a problem rather than a resource for the external electrical grid [7,12].

The limited variations and voltages required in the TF coils allow some options for PS optimizations. For example, traditional PSs could be substituted by contactless systems, known as flux pumps, able to minimize the losses in superconducting circuits in stationary conditions [13].

For the PF PSs, an identified improvement consisted of introducing a buffer of energy to limit the power exchange between the coils and the external grid. In principle, different topologies and technologies are possible. An energy storage was also proposed for the TF circuit at the AC side [14]. However, the most promising solution appears to introduce the energy storage in the DC link of the PF PSs [15] and sometimes of other coils. The technical reasons for that will be clear throughout the paper.

It is evident that these kinds of problems are generally encountered in other energy sources and power conversion applications, where energy storage plays a pivotal role in ensuring stability and performance, becoming more and more essential. Nevertheless, the PF PSs are characterized by peculiar features: while the average energy and the duty cycles can be relatively small (especially in the present experimental plants), the power peaks are extremely high; many fast variations and charge/discharge operations are requested every day. These features suggest that supercapacitors (SCs), with their high power density and rapid charge–discharge capabilities, could be the suitable energy storage device [16–22]. Therefore, SC banks were inserted in support of the tokamak PSs, in particular in DC links between AC/DC and DC/DC converter stages, as is explained in the paper.

After identifying this reference solution, the design challenge consists of minimizing the physical footprint of these DC storage systems while maintaining their functional integrity and reliability. In fact, as the SC banks may be the most expensive and largest part of a new PS system, an excessive size would cancel its potential advantages.

It is important to stress that a good optimization requires using the DC link differently from the standard mode in electronics, where the DC link is designed to operate at a rather constant voltage. In practice, a standard DC link is not a storage device because only a fraction of its energy, which is already small for a traditional capacitor, can be used. On the contrary, the voltage across the SC banks must change between the minimal values to implement the desired scenarios and the safe values for the hardware.

Since the interactions among circuit parameters and the coupling with the other tokamak elements are complex and time-variable, it is rather impossible, or at least impractical, to approach the design and optimization from an analytical point of view. Nevertheless, some models and formulas were developed to provide a starting range for the procedure and to include all the tokamak elements in a circuital model. This model can be used to validate the design. As the primary focus of the study was the DC link optimization, the PS circuits are based on a single H-bridge converter [15].

This paper will show that, for (superconductive) inductive loads, SCs are more advantageous than expected by a simple look at the classical Ragone plot. In fact, the optimization can exploit some specific characteristics and function principles of PF coils. The paper does not explicitly include the optimization of other types of coils that can induce PFs, but are not strictly PF coils, because they have different functions: the central solenoid (CS) [4], the vertical stabilization (VS), the fast radial control (RC), and the divertor (DIV) coils [15,23]. Analogously, the PSs for the non-axisymmetric coils used for error field correction (EFC) and edge-localized modes (ELMs) [23] are out of the scope of this paper, also because they will be addressed in different papers. Nevertheless, it will be explained how the different coil functions imply a different optimization approach and results.

For these reasons, even though the approach is generally applicable to all tokamaks and other nuclear fusion plants, the analysis must be carried out on real cases. This

paper is focused on a last-generation tokamak named the Divertor Tokamak Test (DTT) facility [23,24], under construction in Frascati, Italy, that is also one of the first public–private partnerships in this field [25]. DTT has six PF superconducting coils, which is a sort of standard in tokamaks, and all the other mentioned coils (CS, VS/RC, DIV) [23].

This paper explores innovative strategies for reducing the size of the DC storage stage in PF PS converters by employing SCs arranged in series and parallel configurations. For the first time, the proposed solution involves the shared utilization of the DC storage stage between pairs of PSs. This approach, validated through simulations, leverages the complementary energy demand profiles observed in certain pairs of coils, allowing for a more efficient and compact design. The findings of the study suggest that such an approach not only reduces the overall size of the DC storage stage but also enhances the performance, efficiency, and cost-effectiveness of the system. For example, an optimized power exchange with the grid can reduce other power quality problems affecting the tokamaks such as reactive power, harmonics, flicker, and oscillations. In particular, the huge power flow variations that could be a showstopper for the exploitation of tokamaks as an energy source [6,7,9,12] could be internally managed.

On the other hand, the paper will show some limitations and issues in the approach, such as the difficulty of optimizing the available power, energy, and voltage.

The implications of this research can be extended to several applications in energy storage and conversion technologies, highlighting the importance of innovative design in meeting the complex demands of advanced energy systems.

The rest of the paper is structured as follows. Section 2 presents the background of the operation of PF coils in a tokamak, providing the reference current and voltage scenario for such operations. Section 3 introduces the reasons for the need for energy storage based on SCs in PF coils. Section 4 describes the main parameters to be optimized for the design of the SC banks. Section 5 presents the possible optimization strategies and criteria for the design of the SC banks, with a specific focus on the PF PS characteristics. In particular, Section 6 proposes an effective optimization technique exploiting the complementarity of the power demands of PF coils. Different approaches are possible, but, after presenting them, the optimization is finalized by circuital simulations, taking into account also the effect of other tokamak elements. The main analytical developments to implement such circuital simulations are described in Section 7. Section 8 presents the parameter ranges and the choices for the simulation campaign. The obtained results are summarized in Section 9, clearly showing the advantages of the proposed approach. Finally, some practical considerations and the conclusions drawn from the study are presented in Section 10.

2. Operations of PF Coils in a Tokamak
2.1. Tokamak Magnetic Configuration

A tokamak is a complex architecture designed to confine and control high-temperature plasma using magnetic fields, with the ultimate goal of sustaining nuclear fusion processes [4]. The magnet system of DTT is schematized in Figure 1 (see also [26] for EU DEMO). Among the different types of coils, PFs are essential for shaping and controlling the plasma within the tokamak, necessitating precise and responsive PS systems [15].

The tokamak core is a toroidal (doughnut-shaped) chamber where the fusion reactions occur. This chamber is surrounded by magnetic coils that work together to create the stable magnetic field configuration necessary for plasma confinement. The TF coils produce a magnetic field around the torus in a continuous loop, providing the primary confinement mechanism. However, the stability and precise shape of the plasma are governed by the PF coils. These coils are arranged in different loops that encircle the torus vertically and horizontally, controlling the plasma's cross-sectional shape and position.

PF coils are critical to the operation of a tokamak, as they dynamically adjust the plasma shape and stability. To fulfill this role, PF coils require highly variable current profiles with peaks reaching tens of kiloamperes. Additionally, these coils must handle voltage profiles that span several kilovolts. The ability to rapidly and accurately control

these high current and voltage levels is essential for maintaining the desired plasma configuration and ensuring the overall stability of the fusion process [4,23].
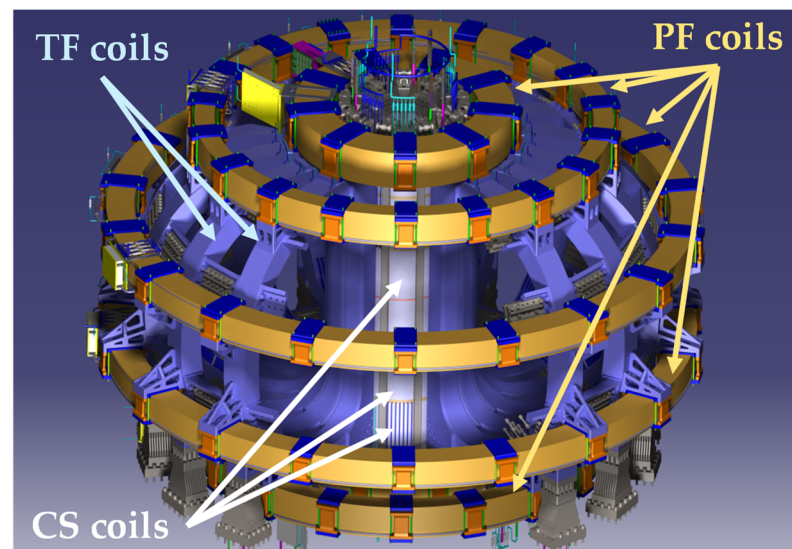

Figure 1. Basic structure of a tokamak (DTT) with emphasis on the magnetic systems.

2.2. Reference Scenario of PF Coils

The prediction of tokamak operations is a very complex and multidisciplinary task, implying the solution of magnetohydrodynamic (MHD) problems [4]. From the PS point of view, tokamak operations are fully described by a "scenario", including the following:

- The profiles of the current for each "active" (supplied) coil.
- A model for the plasma behavior in terms of filaments of equivalent electrical currents.
- The parasitic currents induced in the tokamak "passive" elements (vacuum vessel, walls, and so on), characterized by equivalent circuits with internal inductance (depending on geometry) and resistance (material losses).

In practice, a scenario is characterized by a time-dependent vector containing the current samples in the desired time instants. The voltage evolutions in the same circuits can be derived by modeling the geometric structure of the tokamak poloidal cross-sections and the magnetic interactions among them. All the flowing currents are magnetically coupled by a square matrix $\underline{M}$ containing the mutual inductances among the active coils, the plasma currents, and the passive elements. For the active coils, the voltage to be produced by the PS systems can be derived from the voltage across the coil terminals, subtracting the voltage drops in the corresponding circuit (including DC bus bars, cryogenic transitions, connections, joints, parasitic effects, and so on).

The waveforms in Figure 2 were calculated using such a procedure for the DTT operations. However, to have a reference scenario for the PS design, these waveforms contain more phenomena with respect to standard scenarios where only equilibrium situations are considered. These include such transient phases as plasma breakdown, plasma ramp-up, L-H mode transition, and H-L mode transition. The analyses for these phases were carried out by the CREATE team [27–29] and reprocessed for this paper. Of course, the calculations involved also the other active and passive currents, in particular those in the CS coils, that are not reported in the plots.
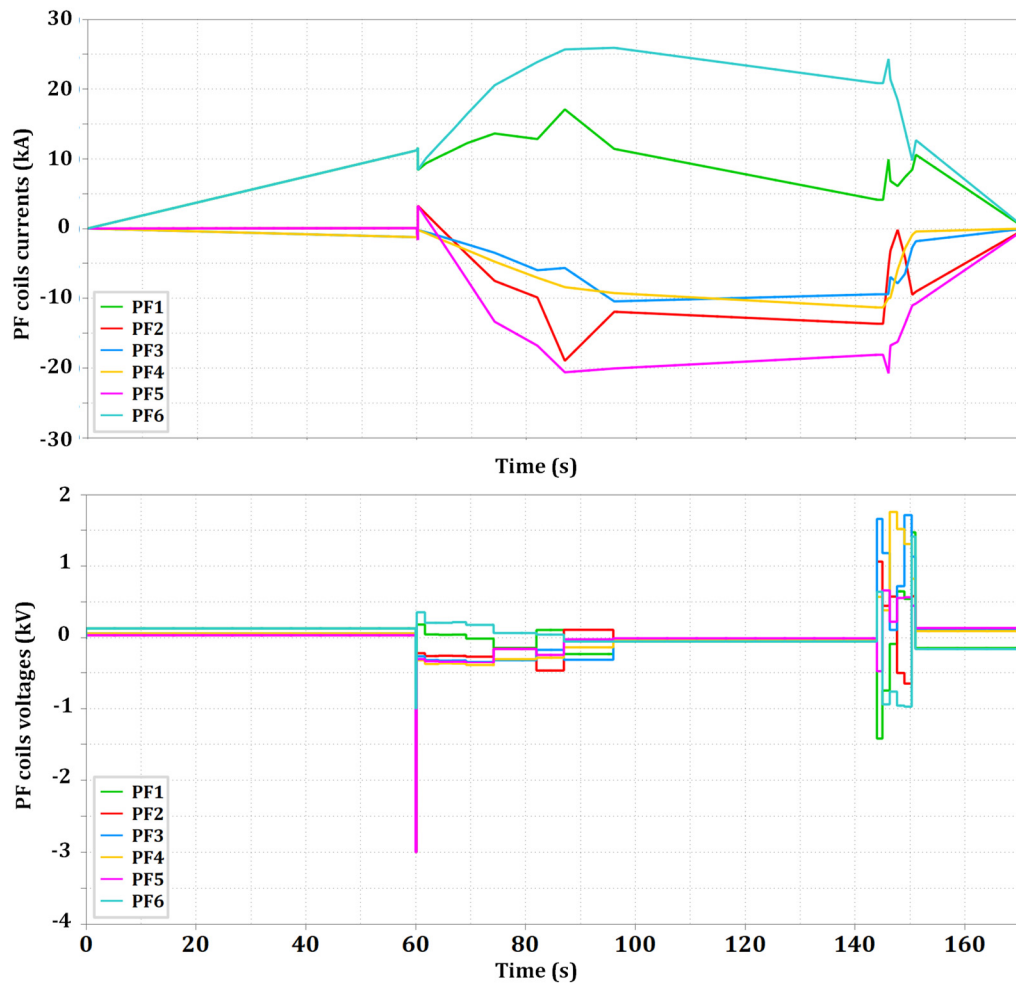
Figure 2. Currents and voltages of the PF coils in the DTT reference scenario, including transient phenomena and phases such as plasma breakdown, plasma ramp-up, L-H mode transition, and H-L mode transition.

Even though other experimental scenarios are possible in DTT [23,28], the scenario in Figure 2 is the most demanding from an electrical point of view and can be used as a benchmark for the design and the optimization.

The waveforms in Figure 2 establish the first specifications for the design of each PF PS, namely, the minimum rated current and voltage. It is important to stress that in many cases the plasma breakdown (occurring at 60 s in Figure 2) is supported by other components in series in the PS circuit, such as a switching network unit (SNU) [30], while for the DTT PF coils, all the phases are implemented by the PS converters.

3. Need for Energy Storage in Tokamak PF Coils

As shown in Figure 3, in the PF PSs, even though the power peaks can be extremely high, the average power needed is relatively small. Moreover, the plant duty cycle is limited, especially in the present experimental plants (it is about 100 s/3600 s in DTT [24]).

To meet the demanding requirements of the PF coils, a robust and efficient storage system is essential, also because the PF coils are only one of the electrical loads necessary to operate an experimental tokamak like DTT [31] or a power station producing energy by nuclear fusion [10]. Such a storage system must be capable of storing large amounts of energy and delivering it precisely when needed.

A standard solution to support the medium/high voltage transmission/distribution lines in past fusion experiments was based on flywheel generators, which are able to provide a high amount of power in short time intervals without affecting the electrical grid

system's stability. This is less common today, because it is difficult to find such devices on the market [14] (actually, some new installations revamp old flywheel generators [32,33]). The other reason is that, approaching tokamaks for energy production, operations are becoming longer and longer, so more flexible technologies are required.
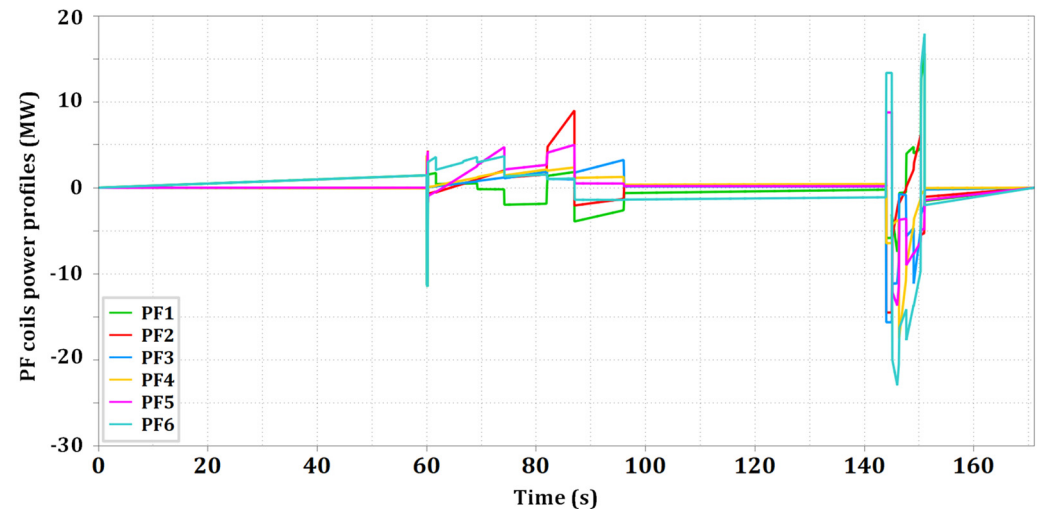

Figure 3. Power delivered to the PF coils in the DTT reference scenario.

A viable alternative currently under study for fusion reactors is the DC storage system based on banks of SCs or other high-capacity energy storage devices that can rapidly discharge and recharge to match the dynamic demands of the PF coils. In this case, the AC/DC converter stage can be classified as a "charger", which can be rated for a power significantly lower than that delivered to the load.

The design and implementation of the DC storage system involve several key considerations. First, the storage system must have a substantial energy reserve to support the peak current and voltage requirements. This ensures that the system can sustain the necessary power output during the most demanding phases of plasma confinement. Second, the system must be capable of rapid response to changes in demand, allowing for precise control over the magnetic field configurations. This is crucial for maintaining plasma stability and preventing disruptions; additionally, the DC storage system must be designed with high reliability and efficiency in mind. Any failure or inefficiency in the power supply could lead to instability in the plasma, potentially causing disruptions or damage to the tokamak. Therefore, advanced power conversion and energy storage technologies are employed to achieve the required performance levels.

3.1. Characteristics and Advantages of SCs

SCs have emerged as a promising energy storage technology, particularly suitable for applications requiring rapid charge and discharge cycles [34]. Key characteristics and advantages of SCs include high power density, long cycle life, wide temperature range, and low maintenance. SCs can indeed deliver and absorb power quickly, making them ideal for buffering short-term power demands, and, unlike traditional batteries, they can undergo millions of charge/discharge cycles with minimal degradation. Furthermore, they operate effectively across a broad temperature spectrum, enhancing their suitability for various environmental conditions. From a maintenance point of view, SCs require less maintenance than batteries, reducing operational costs. For these reasons, they were considered for mobility and renewable sources, but with lower power and energy levels and shorter time scales with respect to the DTT PF PSs [35,36].

The integration of SCs into the DC storage stage between the AC/DC converters and the DC/DC converters can significantly improve the performance and reliability of the PSs

for PF coils. Moreover, SCs can be also utilized in other PSs within tokamaks and other fusion systems.

Of course, SCs do have some drawbacks too. Notably, their equivalent capacitance decays with frequency, becoming almost negligible at frequencies around 100 Hz, while the internal losses increase [37–39]. This limitation necessitates the use of additional filters to interface SCs effectively with power electronics, ensuring that they can still meet the demands of the system without introducing unwanted harmonics or instability. These filters are crucial for maintaining the PSs' overall performance and reliability, as they mitigate the effects of the SC frequency-dependent characteristics [19].

Modeling an SC with precision in simulations is a complex and non-trivial task due to the intricate behavior involving numerous parameters and complex phenomena [40]. Even though the authors are experimentally and theoretically characterizing such phenomena [40], the time scale of the analysis is compliant with the adoption of a simplified model for the purposes of this work in order to focus on the energy balance analysis, without considering transients associated with individual components. The entire SC bank was simulated using a single capacitance, representing the total bank value, in series with a resistance reflecting the equivalent series resistance (ESR) of the bank. This approach streamlined the simulation process while still capturing the essential dynamics of the energy storage system.

The Ragone plot is a typical tool used to compare energy storage technologies based on their power and energy densities [41,42]. A Ragone plot with the essential information for this paper is sketched in Figure 4. The ellipses in Figure 4 denote the most relevant families of storage technologies. This representation clarifies that SCs cover a zone complementary to other technologies, offering a trade-off between the high specific energy of batteries and the high specific power of traditional capacitors. Lithium-ion capacitors (LICs) are SCs with a sort of battery-like electrode to extend the energy capabilities and then the covered zone.
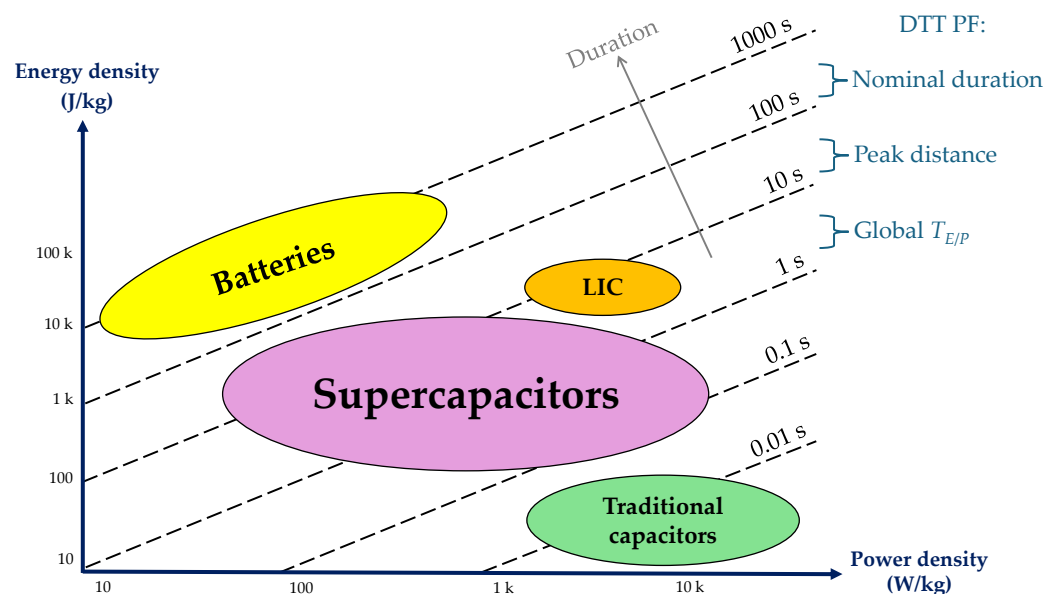

Figure 4. Ragone plot comparing the main energy storage technologies and some typical durations of their operations. To support the analysis of this paper, some characteristic times of the DTT PF PS system are also reported, to be discussed in the following paragraphs.

The dotted lines in Figure 4 summarize the characteristic durations of the operations having the corresponding powers and energies. According to this tool, SCs operations should be limited to a few tens of seconds.

3.2. A Specific Use of the Ragone Plot

However, the Ragone plot is often misinterpreted. To introduce the analysis well, it is important to stress that an energy storage system can work also outside its zone, but, in this case, it would be oversized either in terms of power or in terms of energy. Nevertheless, it could be suitable in terms of the number of cycles, costs, or other aspects.

The duration to be considered is not only that of the scenario, but a shorter equivalent value could be adopted due to several factors. The most relevant is the type of load (dissipative or inductive) and the capability to recover the energy from the load and from the charger by supporting a huge number of fast charge/discharge cycles [43]. In this case, the equivalent duration is approximately the time between two positive power peaks.

On the other hand, the SC voltage cannot be considered constant during the operations, affecting both the coordinates of the Ragone plot. This always must be included in the optimization, even if it complicates the calculations due to the variable voltage requirements (see Figure 2).

Therefore, while the scenario is nominally 100 s for the DTT plasma and about 160 s for the DTT PF coils, the maximum interval between positive power peaks is in the interval $100 \div 140$ s in Figure 3, resulting in about 40 s. An input charger with a rating of a few megawatts can further reduce this interval by contributing to the power required by the scenario and thus limiting the SC voltage discharge.

For these reasons, the use of DC storage and SCs would be appropriate for tokamak PF systems. Another paper will develop this discussion and will extend it also for TF, CS, VS, RC, DIV, EFC, and ELM coils and their operations.

4. Possible Optimization Parameters with Their Constraints

Having assessed that PF PSs would benefit from an energy storage based on SCs, the design challenge consists of optimizing its dimensions and costs together with its power demand from the grid. In fact, the SC banks may be the most expensive and largest part of the PS system. A simple design based on peak requirements would cancel any potential advantage in terms of cost and performance. In practice, it is necessary to solve an optimization problem under strongly variable and complex loads.

In typical commercial technologies for energy storage applications, a single SC cell has a capacitance on the order of thousands of farads but can sustain a voltage on the order 2–3 V. Therefore, the practical implementations are always based on the series (and parallel) of multiple cells. For this reason, manufacturers usually provide assembled modules with voltages on the order of tens or hundreds of volts (for example, 16, 48, 54, 64, or 160 V). For the specific case of PF PSs, these voltages are still insufficient and, in addition, the required current (power) and energy can be attained only by packs (banks) of SC cells or modules. Some manufacturers propose racks of modules including some management, control, and cooling systems. Racks are useful for specific applications such as grid storage, but their fixed voltage does not allow a flexible design optimization.

The first step in PS design consists of the choice of a topology. For the purpose of this paper, a single H-bridge based on IGBTs with a single SC DC link can be considered. Figure 5 shows a block scheme of the PS topology for a single PF coil that will be used for the optimization and for the circuital simulations.

In the final design, more IGBTs/bridges in series/parallel, or the split of the DC link in more SC banks connected to a portion of the necessary H-bridges, could have practical benefits [44]. However, these details would not affect the dimensions of the SC–DC link to be optimized and the following analysis. A slightly different situation occurs when an SC module and a small converter are combined in a basic unit to be connected in series/parallel to reach any value of voltage/current [14]. This has the advantage of focusing on the design of a single unit [14] but is constrained to discrete values, resulting in fewer degrees of freedom in achievable optimizations. For this reason, the adoption of a large DC link, not related to any particular SC model, is preferred for the analysis.
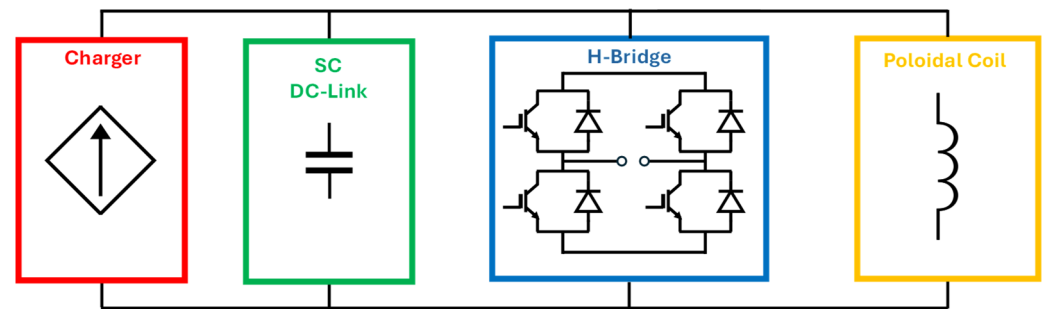
Figure 5. General topology of the PF coil PS used for the design and optimization.

To have a good balance, the banks must consist of cells/modules from the same family and must contain the same number, N_s, of SCs in series in each of the N_p parallel branches, thus resulting in being fully defined by the dimensions $N_s \times N_p$.

It is commonly accepted in all the references that the model of a group of series/parallel cells can be extended from the model of a single cell. This is not strictly sound according to the circuit theory for more complex models, but it is, rather, applicable to a simplified model equivalent capacitance plus ESR. In particular, this simplification is valid if all the assembled cells/modules are identical. This is not valid in real cases due to the component tolerances. Another aspect to be considered is that the application of the standard formulas for linear circuits is not applicable under the non-ideal phenomena observed in SCs [40]. However, manufacturers usually include in the commercial modules/cabinets specific systems to balance the tolerances [45,46]. This supports the simplification, but, on the other hand, slightly modifies the SC equivalent circuit. Therefore, the tolerances are expected to be compensated in the estimation of the bank size, and they could be covered in the assumed safety margins. The absence of direct characterization of modules and packs is probably related to the difficulty of finding a specific instrument to perform it. Nevertheless, a verification is presented in [38] for two SC cells and in [46] for four cells with balancing.

Therefore, the parameters to be considered for the optimization are as follows:

- Base SC cell or module. This is important to identify the unitary voltage and capacitance, but also the ESR intrinsic to it [47].
- Number of series N_s and/or parallel N_p cells/modules.
- Maximum current requested to supply the load coils in the desired scenario $I_{L\max}$. As the peak current of the SC cells is extremely high (on the order of 1000 A), this parameter is normally well satisfied when the other ones are optimized.
- Maximum voltage $V_{\max}$ across the DC link. This is not a trivial parameter, because the voltage of the DC link can change during the operation to fully exploit the stored energy. Of course, it cannot exceed the maximum rated values of the SC cells and of the rest of the hardware. Normally, the voltage limitations are not due to the number of SC cells that can be placed in series (what is reported in the datasheets for modules is due to the insulation of the diagnostic systems), but to the other components as the IGBTs. It is a design choice whether to select as $V_{\max}$ the maximum value requested by the load coils during the scenario or the maximum value allowed by the hardware. The energy is higher with the latter choice.
- Minimum voltage $V_{\min}$ necessary to drive the currents in the desired scenario(s). In fact, a PS converter can operate only if the voltages across the semiconductor switches exceed their turn-on values. These minimum voltages are not trivial parameters, because the voltage of the DC link can change during the operation to fully exploit the stored energy. As explained in the next section, SC manufacturers usually provide characteristics for cycles not discharging below $V_{\max}/2$.
- Peak power requested to supply the load coils in the desired scenario(s). For the properties of the Ragone plot, using SCs, this parameter normally is also well satisfied when the other ones are optimized.

- Maximum energy stored or storable in the DC link E_{DC}. It seems an immediate parameter given by the time integral of the power during the scenario, but it is not the optimal operating mode for pulses longer than some seconds. The actual value must be selected in compliance with the maximum input power demand from the grid.
- Maximum input power demand from the grid $P_{gridmax}$ (and related charger rating). In principle, this power can even be zero if the scenario is completely driven by the energy in the DC storage. This can lead to a simplification for very short operations [17]. However, as some form of charger must be present, it generally makes sense to exploit its contribution.

All these parameters are discussed in the next section. Here, it is worth noticing that they are not independent. The most important relationship is that between V_{max} and E_{DC}, established by the well-known formula

$$E_{DC} = \frac{1}{2}CV_{max}{}^2 \tag{1}$$

Better optimization performance could be achieved by releasing or relaxing the constraints among parameters. A higher energy density can be obtained if the DC storage is based on LICs [21] or hybridized with batteries [35,36]. A separated charger can provide a higher V_{max} specifically for short ramps [17]. A deeper SC discharge can be obtained by inserting a further stage with a boost converter between the SC bank and the H-bridge. An offset to V_{max} not depending on (1) can be added by an H-bridge fed by standard capacitors in cascade with the H-bridge fed by the SCs [22]. Further ideas to reduce the interdependence among parameters are proposed in the next sections. However, none of these solutions appears so advantageous in general cases as to justify its additional costs or complications. These aspects should be holistically investigated in future works.

5. Optimization Strategies and Criteria

The assessment of all these parameters using an analytical approach is rather impossible, or at least impractical [48]. Sections 8 and 9 address the problem by simulations. However, some formulas were derived to have guidelines to approach the problem, as presented in this section.

5.1. Available Optimization Formula for PF Coils

Considering the SC and the converters as ideal, the most simplified balance consists of transferring all the energy stored in the SC to the load. So, the DC energy, E_{DC}, must be higher than that storable in the load, E_L:

$$E_{DC} \gg E_L \tag{2}$$

The energy in the SC can be derived from V_{max} by (1). However, it is useful to report that the SC capacitance also depends on voltage, with a mostly linear behavior [49,50] (though more refined approximations could be proposed [51,52]):

$$C(V) = C(V_{ref}) + k_v[V - V_{ref}] \tag{3}$$

This effect is never reported in manufacturers' datasheets but is commonly observed in experimental characterizations [49,50]. For this reason, (1) can be used to retain the effect in (3) as a safety margin for design.

If the load is limited to the coil, its (magnetic) energy is simply due to its autoinductance, L:

$$E_L = \frac{1}{2}LI_{max}{}^2 \tag{4}$$

Table 1 reports the values of auto-inductances of the DTT PF coil corresponding to diagonal entries of the inductance matrix, $\underline{\underline{M}}$.

Table 1. Nominal auto-inductances and possible magnetic energy storable in the DTT PF coils. The energy calculated using (4) is compared with the E_s obtained by the complete MHD model.

PF Coil	L	E_L	E_s
PF1	454 mH	80 MJ	47 MJ
PF2	298 mH	65 MJ	54 MJ
PF3	690 mH	46 MJ	53 MJ
PF4	690 mH	269 MJ	66 MJ
PF5	298 mH	77 MJ	88 MJ
PF6	454 mH	185 MJ	100 MJ

However, the actual energy also contains other contributions that can be calculated by integrating the powers in Figure 3, as shown in Figure 6. In this way, a scenario energy variable with time $e(t)$ is obtained (here and in the following, the lowercase letters denote a time-dependent behavior):

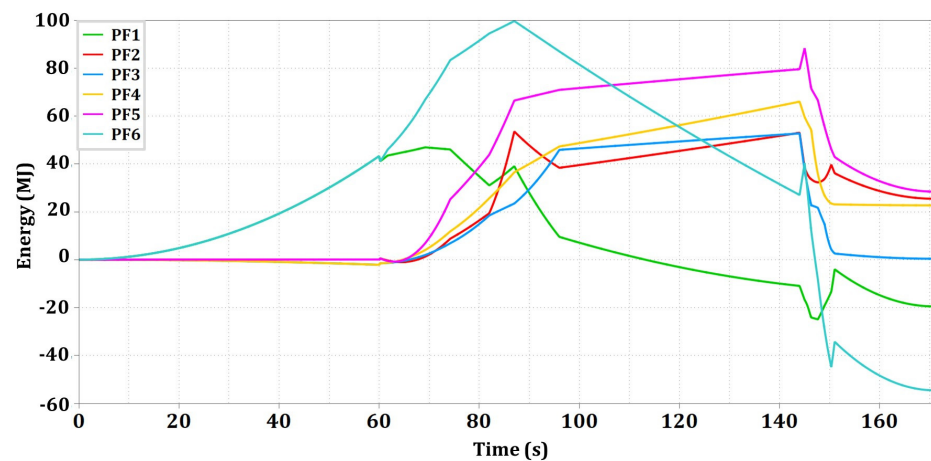$$e(t) = \int_0^t p(\tau)d\tau \tag{5}$$

Figure 6. Energies delivered to the PF coils in the DTT reference scenario.

Figure 6 neglects the negative energies at the end of the operation, because they derive from the basic idea of discharging all the coils in the same time interval (see Figures 2 and 3), which may give more energy back to some coils with respect to others. This would be corrected when the scenarios are conceived, also considering this aspect.

An interesting single parameter characterizing the scenario energy consists of its maximum over time:

$$E_s \overset{\text{def}}{=} \max_t \{e(t)\} \tag{6}$$

The values of E_s and E_L coincide for a single coil without mutual interactions.

The definition of E_s allows the introduction of the new concept of efficiency of the DC storage, that is, the portion of available energy that is actually used for the load:

$$\eta_{DC} \overset{\text{def}}{=} \frac{E_s}{E_{DC}} \tag{7}$$

It is important to stress that, while a high η_{DC} means a full exploitation of the SC bank, on the other hand, a lower value can provide a safety margin that could be useful to compensate for unexpected and not considered effects (for example, the internal losses and drops in the semiconductors).

The values of energies estimated by the different approaches are compared in Table 1. The use of E_{DC}, derived by the complete MHD model, provides a remarkable reduction for the estimation of the energy flowing in the PS circuits, and thus, a potential increase in the achievable efficiency.

5.2. Minimum Voltage for DC Link Design

A more refined approach considers also a minimum voltage of the SC bank V_{min} that can be inserted in the model, yielding the following (either E_s or E_L could be used):

$$\frac{1}{2}CV_{max}^2 - E_s > \frac{1}{2}CV_{min}^2 \tag{8}$$

With the introduction of V_{min}, the efficiency η_{DC} depends on the V_{min} selected in the design:

$$\eta_{DC} \cong 1 - \left(\frac{V_{min}}{V_{max}}\right)^2 \tag{9}$$

It clarifies the importance of having a large range of $V_{min} \div V_{max}$ that is strongly related to η_{SC}.

The value of V_{min} must have the following characteristics:

1. Higher than the voltage necessary to drive the load, corresponding to the voltages in the scenario in Figure 2, plus the voltage needed to keep the IGBT in conduction.
2. Higher than a value that is considered safe or more appropriate for the SC bank.

Since the latter value is not well defined, a simplified approach could be used.

5.3. Simplified Approach Based on Half-Voltage Cycles

A good approach consists of the adoption of a V_{min} corresponding to half of the maximum voltage of the SC bank ($V_{min} = V_{max}/2$). The main reason for that is the use of charge/discharge cycles between V_{max} and $V_{max}/2$ to define the SC specifications [40,53]. Moreover, LICs have a specific requirement to operate in this range, because they could be irremediably damaged if discharged below a certain threshold, close to $V_{max}/2$ [54].

The half-voltage approach has the advantage of simplifying the calculations in (8), leading to an explicit requirement for the capacitance to be selected for the SC bank:

$$C > \frac{4}{3}L\frac{I_{max}^2}{V_{max}^2} \tag{10}$$

Once the bank capacity is known, together with its V_{max}, the bank energy can be immediately calculated by (1). The capability of generating the I_{max} should be verified, but it is normally satisfied. The simplified formula (10) does not take into account the effect from (3) that can be kept as a further safety margin.

With this approach, η_{DC} is fixed to 75%, which is also the used energy with respect to the available one. Moreover, (10) does not ensure automatic compliance with the first condition at the end of Section 5.2, so it shall be independently verified.

5.4. Approach Based on the Scenario in the Time Domain

The previous approach limits the efficiency to 75%, while an SC discharge deeper than 50% is not critical, even if it would lead to a partial reduction in the lifecycle.

The best balance of energy not involving the grid can be obtained when the energy delivered to the load is not sufficient to lead the SC bank to a voltage lower than that requested by the scenario:

$$\frac{1}{2}CV_{max}^2 - e(t) > \frac{1}{2}Cv(t)^2 \tag{11}$$

In this case, in order to include all the tokamak effects, the load energy is that shown in Figure 6. The resulting model can be implemented easily in simulations:

$$C > \max_t \left\{ \frac{2e(t)}{V_{\max}{}^2 - v(t)^2} \right\} \tag{12}$$

Table 2 summarizes the values reached by *C* for each PF coil. This is an optimistic value for the bank capacitance that does not include some losses' effects.

Table 2. Results of bank design obtained by optimization in time domain.

PF Coil	Minimum *C* from (12)	Minimum E_{DC} from (13)	Related η_{DC}
PF1	39 F	63 MJ	75%
PF2	10 F	58 MJ	92%
PF3	11 F	68 MJ	78%
PF4	12 F	72 MJ	91%
PF5	16 F	92 MJ	96%
PF6	62 F	100 MJ	100%

As for (10), once the bank capacity is known, together with its $V_{\max}$, the bank energy can be immediately calculated by (1):

$$E_{\mathrm{DC}} > \max_t \left\{ \frac{e(t)}{1 - \left[\frac{v(t)}{V_{\max}} \right]^2} \right\} \tag{13}$$

The results are also reported in Table 2. Finally, the capability of generating the $I_{\max}$ should be verified, but it is normally satisfied.

If the time instant corresponding to E_{s} is the same as the minimum of $V_{\min}$, (12) would result in an efficiency close to the value given by (9). This is the most common case, but in principle, the voltage required by the scenario could determine the instant of the maximum in (13), leading to a higher design capacitance. In this case, it is always as follows:

$$\eta_{\mathrm{DC}} < 1 - \left(\frac{V_{\min}}{V_{\max}} \right)^2 \tag{14}$$

This means that the approach based on a scenario in the time domain can lead to smaller banks with higher efficiency, even though efficiency could potentially be out of the design choices. However, this situation never occurred for the DTT PF coils.

5.5. Loss Compensation

The previous formulas were derived under the assumption of an ideal (lossless) system. The real behavior is affected by several causes of losses: SC ESRs, parasitic elements on the AC or DC sides (such as cables, bus bars, and connections), drops in the converters' semiconductors, passive elements such as the vessel and the walls, and the plasma equivalent resistance. Modeling such contributions is rather impossible, because they include phenomena that are dependent on time, frequency, current, voltage, and so on. The knowledge of the complete model of the scenario like in Figure 2 allows us to cover the effects due to the tokamak, while the rest of the effects can be only predicted.

A good rule of thumb could be to have an input power, P_{gridmax}, able to compensate for the maximum power and/or energy during the operations. These can be estimated from Figures 4 and 6, taking into account that high power peaks for short intervals can be

managed. Based on these considerations, P_{gridmax} in the range $1 \div 3$ MW was selected as the starting point for the following analyses.

6. Complementarity in Power Demands of PF Coils

The previous discussion was focused on PF systems but is mostly applicable to other coils. In the following, the specific characteristics of PF systems will be exploited. In tokamak systems, different PF coils may exhibit complementary energy demand profiles. This means that while some coils require high power input, others may have lower power demands or even release energy back into the system, as shown in Figure 2 for the DTT case. By analyzing these demand profiles, it is possible to design a shared DC storage system that optimally balances the energy requirements across multiple coils.

Figure 7 shows the total power delivered to the load coils by all the PF PS systems. This power is integrated over time to show, in Figure 8, that most of the energy involved in the operations can be recovered because the effective losses in the process are very limited, especially if compared with the peak powers. For completeness, it is necessary to report that a part of the power goes to the plasma and to the passive elements, while a contribution is also provided by the CS coils. Probably, only the first DTT experiments could provide a quantification of the losses. However, even an incomplete recovery of the energy necessary for the tokamak operations is a relevant achievement.
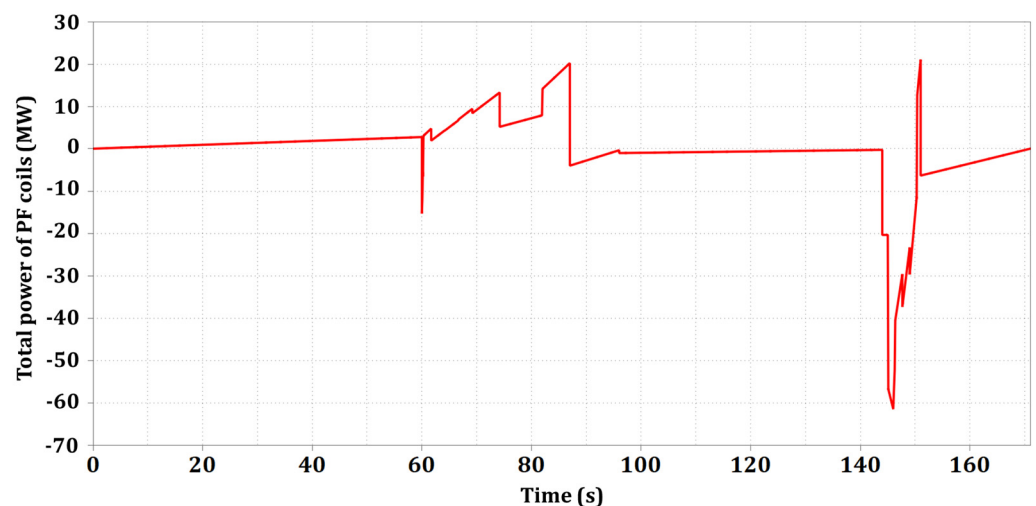

Figure 7. Sum of the six instantaneous powers of the six PF coils shown in Figure 3.
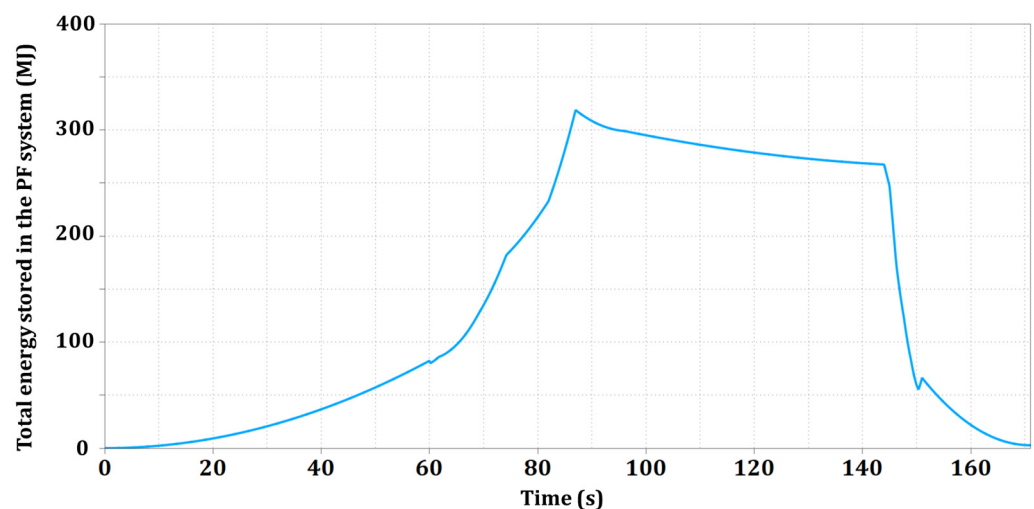

Figure 8. Total energy stored in the load coils and equivalent mutual couplings.

Figures 7 and 8 help to clarify that the total power is lower than the sum of the rated powers of each PS in Figure 3, suggesting that a common storage could reduce the overall power demand. This is due to a phenomenon of complementarity in the power demands of PF coils. One of the novelties of this paper consists of the exploitation of such a phenomenon.

This characteristic is evident in DTT, leading to the significant findings reported in Section 9. Moreover, even though it is not easy to collect data for all the cases, some preliminary observations of the current scenarios of other tokamaks suggest that the approach proposed in this paper could be applicable to other situations. Figure 9 presents a relevant example: the first reference single-null scenario of JT-60SA [55], the largest superconducting tokamak operating in the world. In Figure 9, the coils are named as in DTT, whereas in JT-60SA, they are classified as "equilibrium field coils" with a different numbering [55]. These JT-60SA coils are presently supplied by thyristor bridges without a DC link. A future paper will extend this analysis to other tokamaks and configurations.
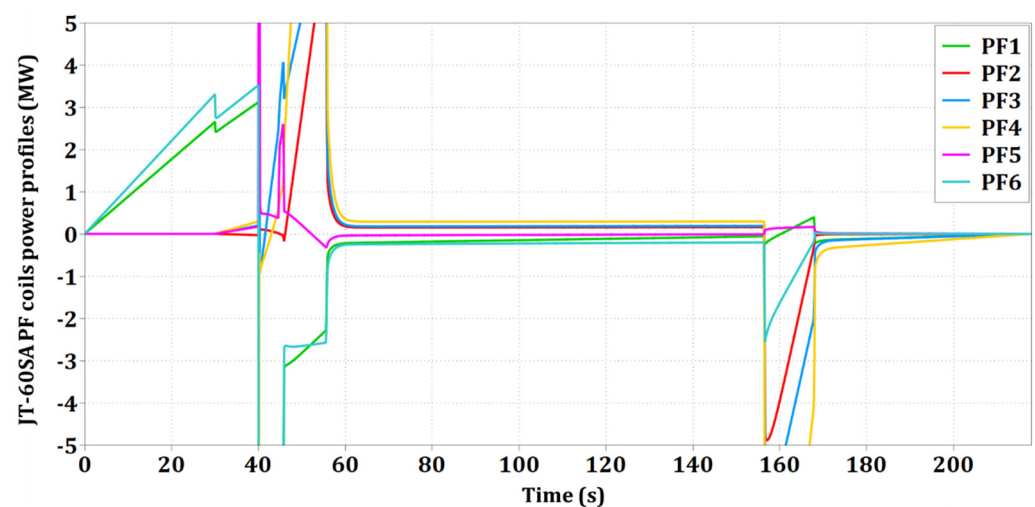

Figure 9. Example of complementarity in the powers delivered to the PF coils in the JT-60SA reference scenario [55] (names of coils are modified to coincide with the DTT ones).

It is important to stress that the optimization moves from scenarios, such as those exemplified in Figures 2 and 9, that were conceived by the plasma physicists independently of any possible optimization of the electrical power or energy. Therefore, the results could be even more significant in the future, with an integrated approach considering these aspects from the beginning.

The concept of complementary power and energy profiles is crucial to optimizing the design of DC storage systems. By leveraging the complementary profiles, it can reduce the footprint of the DC storage while maintaining the required performance.

Equivalent Parameters for Shared DC Links

An observation of the peaks in Figures 7 and 8 allows the introduction of a new global equivalent time, $T_{E/P}$, based on these peaks:

$$T_{E/P} \stackrel{\text{def}}{=} \frac{\max\limits_{t}\left\{\sum_{n=1}^{6} e_{sn}(t)\right\}}{\max\limits_{t}\left\{\sum_{n=1}^{6} p_n(t)\right\}} \cong 5 \text{ s} \tag{15}$$

This time can be compared with the durations in the Ragone plot, as shown in Figure 4, showing again, in a different way, that SCs are the perfect solution to optimize the DTT PF system.

Formulas (12) and (13) can be extended to a DC link with a capacitance C shared among coil PS circuits, each having its own $v_n(t)$ and $e_n(t)$ but the same V_{max}:

$$C > \max_t \left\{ \frac{2\sum_n e_n(t)}{V_{max}^2 - \max_n \left\{ v_n(t)^2 \right\}} \right\} \tag{16}$$

$$E_{DC} > \max_t \left\{ \frac{\sum_n e_n(t)}{1 - \max_n \left\{ \left[\frac{v_n(t)}{V_{max}} \right]^2 \right\}} \right\} \tag{17}$$

These formulas seem complex but can be easily implemented in software simulations.

The performances achieved by a shared DC link having an energy E_{DC} can be quantified by introducing new definitions of efficiency. The first one extends (7) to the global efficiency of the shared DC link by comparing it with the total energy of all the shared circuits:

$$\eta_{DC} \stackrel{\text{def}}{=} \frac{\sum_n E_{sn}}{E_{DC}} \tag{18}$$

Alternatively, the sharing process between the PSs of different coils, each with bank energy E_{DCn}, could be assessed by the following ratio:

$$\eta_{sharing} \stackrel{\text{def}}{=} 1 - \frac{E_{DC}}{\sum_n E_{DCn}} \tag{19}$$

In both these definitions, the efficiencies may exceed 100%.

7. Models for Circuital Simulations

To evaluate the optimal balance between the size of the DC energy storage and the peak power drawn from the grid, an electrical model must be implemented in a software tool for power electronics. The specialized tool PLECS was used to simulate the block diagram in Figure 5 for each PF coil, including all the components necessary for the operations but not reported in Figure 5. The most relevant principles of the developed model are described in this section.

The implementation of the scheme in Figure 5 in a software environment for circuit simulation can adequately reproduce the behavior of the tokamak PS system only by adopting a method to model the effect of the mutual couplings. Without these couplings, the ratings of the components would appear higher, resulting in an oversized design. An inductance matrix $\underline{M}$ with any number N of rows/columns is not available in any software for circuits. Anyway, the computational burden of only six coupled PS circuits is already unmanageable, while an optimization process requires many simulations. Therefore, it is fundamental to introduce a method to emulate all the effects through a simplified approach.

In the most general case, the vector, $\underline{v}(t)$, of the voltages across all the PF coils and all the other poloidal cross-section elements can be obtained by the vector, $\underline{i}(t)$, of the impressed currents through the following formula:

$$\underline{v}(t) = \frac{d\left[\underline{\underline{M}}(t) \times \underline{i}(t) \right]}{dt} \tag{20}$$

In this formula, the mutual inductance matrix, $\underline{\underline{M}}$, is also time dependent. This is not manageable by a circuital simulator.

If the voltage and current profiles are known for the coil under analysis, the situation can be modeled using a standard system with constant mutual inductance. To this aim, the voltage across the k-th PF coil can be expressed as

$$v_k(t) = \sum_{n=1}^{N} M_{kn} \frac{di_n(t)}{dt} \tag{21}$$

where M_{kn} is the mutual inductance between the k-th PF coil and the n-th element (with $n = 1 \div 6$ for the PF coils and $n = 7 \div N$ for the passive elements) and $i_n(t)$ is the corresponding current. The auto-inductance and the current of the considered coil can be denoted with L_k and $i_k(t)$, respectively.

Instead of considering all the N elements, a coil is magnetically coupled to a single fictitious auxiliary coil having a controlled current source in series $i_A(t)$. In this case, (21) can be rewritten as

$$v_{kA}(t) = L_k \frac{di_k(t)}{dt} + M_{kA} \frac{di_A(t)}{dt} \tag{22}$$

The two previous formulas provide the same voltage across the coil at every time instant $v_{kA}(t) = v_k(t)$. Hence, the controlled current $i_A(t)$ is dynamically determined through a simple control loop that forces the desired equality in (22). Integrating and solving for $i_A(t)$, the condition becomes

$$i_A(t) = \frac{1}{M_{kA}} \left(\int_0^t v_k(\tau) d\tau - L_k i_k(t) \right) \tag{23}$$

Since $v_k(t)$, L_k, and $i_k(t)$ are always known, all the mutual couplings can be emulated by controlling the current in the auxiliary inductor using (23). The value of M_{kA} (like the L_A of the auxiliary coil) can be arbitrarily chosen, provided that it is coherent with the other circuit parameters. Figure 10 depicts the block scheme implementing the previous algorithm for mutual coupling contribution.
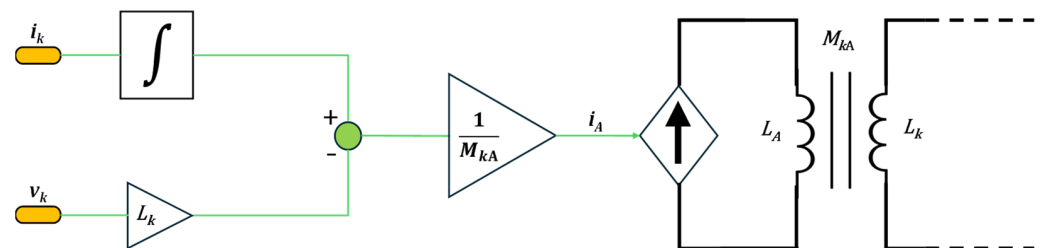

Figure 10. Block scheme of the control algorithm to emulate the mutual coupling contribution.

Figure 11 schematizes the logic emulating the behavior of the charger with a controlled current source. The charger supplies current whenever the DC link voltage drops below a reference threshold, but without overcoming the imposed limit on P_{gridmax}. The threshold control includes a hysteresis band between the $V_{\max}$ and ($V_{\max} - 10$ V). When the charger is activated, it supplies the maximum current that it can provide based on the fixed P_{gridmax} and $V_{\max}$. A more refined control could limit the charger current based on the expected (feedforward) needs of the scenario.

As mentioned, a simplified SC model (capacitance and ESR) can be adopted for the SC bank to focus on the energy balance analysis.

Figure 12 depicts the block diagram of the H-bridge control algorithm. Starting from the load current error, a PI regulator generates the modulating signal, which is compared with a triangular carrier at switching frequency. The direct output of the comparator provides the driving signal of the first diagonal of the bridge, while the negated generates the one for the second diagonal.
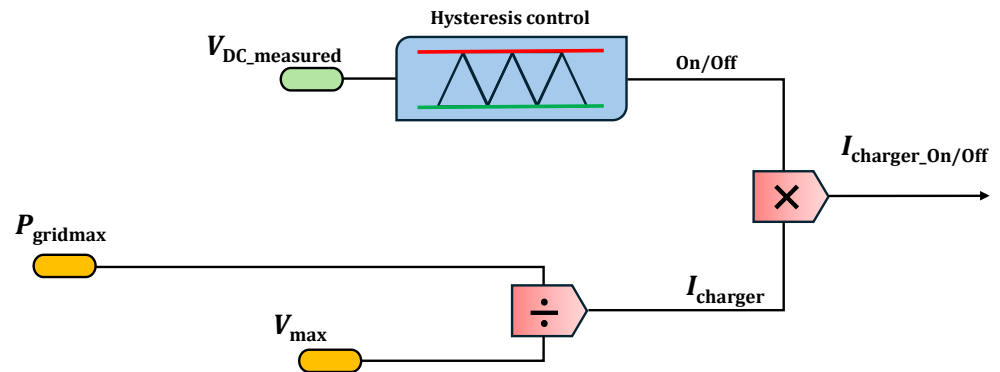
Figure 11. Logic of the controlled current source implementing the charger in circuital simulations.
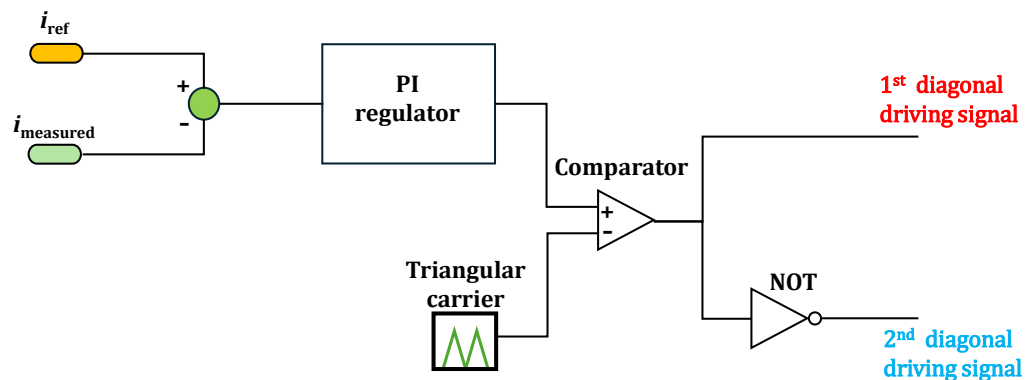

Figure 12. Block scheme of the H-bridge control.

8. Simulation Campaign

Even though some preliminary indications on the best compromises were obtained by Formulas (16) and (17), the useful optimizations must be verified by simulations.

For the simulations, $V_{\max}$ = 1.8 kV or 3.5 kV was selected, to allow the use of commercial IGBTs with performances at the switching frequency suitable for the application. For instance, 3.5 kV can be sustained by a single 6-kV IGBT for railway applications, by a series of three IGBTs having the very common rating of 1.7 kV, and so on.

The PF PSs, each with an installed power up to 90 MW, can operate with an input power lower than 3 MW. In particular, the optimizations were analyzed under three different limits of P_{gridmax} (the input power factors are negligible in this analysis):

1. Maximum 1 MW.
2. Maximum 2 MW.
3. Maximum 3 MW.

Under each of these three different power limits, the study compared two opposite conceptual topologies:

1. Independent DC links.
2. Shared DC links.

In the first case, each PS operated with its own dedicated DC link (DC storage bank). This configuration served as a baseline for comparison. The second case, schematized in Figure 13, exploits the benefits of a DC link shared among PSs feeding different PF coils.
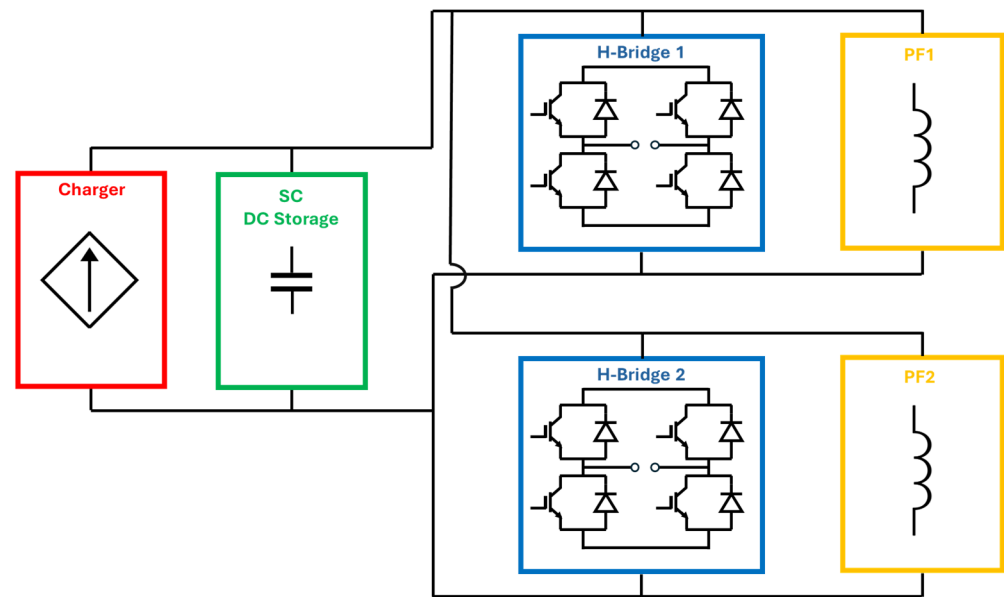
Figure 13. Basic circuit in the case of a shared DC link (PF1 and PF2 pairs as an example).

Choice of the Possible Pairs

As the powers and energies in some time instants (see Figures 7 and 8) are still relevant, a large energy storage involving several PF coils would have limited efficiency. In particular, the preliminary simulations showed that sharing a DC link among all the PF PSs would lead to limited advantages, especially if compared with the related engineering problems. On the other hand, connecting two PSs at the opposite sides of a common DC link has evident advantages in terms of layout. Then, the analysis was focused on combining pairs of PF coils. Starting from the power profiles of the six PF coils shown in Figure 3, the possible pairs were examined to identify the best options.

Trying to combine the power profile dynamics in order to mitigate as much as possible either the average power drawn from the DC storage or the power variations, the most logical pairs in terms of possible sharing of the DC storage bank are as follows:

1. PF1 and PF2 (PF1–PF2).
2. PF3 and PF4 (PF3–PF4).
3. PF5 and PF6 (PF5–PF6).

9. Main Simulation Results

9.1. Results Achieved by Pairing

The advantage of pairing is clearly exemplified in Figure 14, where the voltage of the DC link of the PF2 PS (17 F at 3.5 kV) is compared between the case in which it is connected individually to PF2 and the case in which it is shared with PF1. In the first case, the DC link voltage decays to zero very quickly due to the power demand of PF2 (that could not be followed with too low a voltage), while this does not happen when PF1 compensates the power, much more than the distribution grid could do.

The main results of the simulation campaign are summarized in Table 3. For each cell, it specifies the following:

1. The capacitance value of the storage.
2. The nominal peak voltage of the DC link.
3. The total energy stored in the bank.

Some PF coils, individually, would need a peak voltage of 1.8 kV, but, when considering the shared DC link case, the bank must be sized for the highest peak voltage needed by the PF coils of the pair (i.e., 3.5 kV). The coupling between PF6 and PF1 has not shown

benefits in terms of energy and dimensions, so it is better to exploit the economies of scale of designing them like the others; this is also a safety margin for operations.
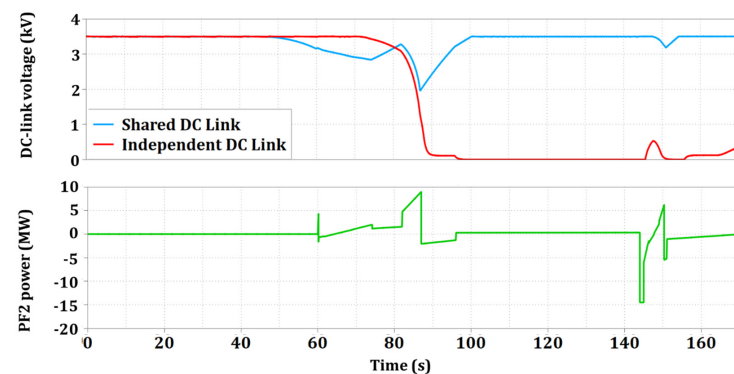

Figure 14. Comparison between the case in which the PF1 and PF2 PSs share the DC storage and the case in which the same DC storage only feeds the PF2 PS.

Table 3. Summary of the differences between the voltage, capacitance, and energy of SC banks in the case of independent and shared DC links.

	P_{gridmax} = 1 MW for Each Coil		P_{gridmax} = 2 MW for Each Coil		P_{gridmax} = 3 MW for Each Coil	
	Independent DC Links	Shared DC Links	Independent DC Links	Shared DC Links	Independent DC Links	Shared DC Links
PF1	1.8 kV 68 F 110 MJ	3.5 kV 30 F 184 MJ	1.8 kV 58 F 92 MJ	3.5 kV 17 F 104 MJ	1.8 kV 44 F 70 MJ	3.5 kV 15 F 92 MJ
PF2	3.5 kV 35 F 215 MJ		3.5 kV 34 F 209 MJ		3.5 kV 30 F 184 MJ	
PF3	3.5 kV 28 F 172 MJ	3.5 kV 60 F 368 MJ	3.5 kV 25 F 154 MJ	3.5 kV 55 F 337 MJ	3.5 kV 18 F 110 MJ	3.5 kV 40 F 245 MJ
PF4	3.5 kV 32 F 196 MJ		3.5 kV 28 F 172 MJ		3.5 kV 22 F 135 MJ	
PF5	3.5 kV 55 F 337 MJ	3.5 kV 38 F 233 MJ	3.5 kV 55 F 337 MJ	3.5 kV 30 F 184 MJ	3.5 kV 25 F 154 MJ	3.5 kV 25 F 154 MJ
PF6	1.8 kV 155 F 233 MJ		1.8 kV 120 F 260 MJ		1.8 kV 105 F 176 MJ	

Table 3 provides significant insights into the advantages and limitations of sharing DC links. One of the most notable findings was the substantial benefits observed for the coil pairs PF1–PF2 and PF5–PF6:

- For PF1–PF2, the shared storage configuration could potentially halve the size required for the storage bank.
- For PF5–PF6, the reduction in storage requirements was even more pronounced, with a potential decrease by about two-thirds.
- On the other hand, the pair PF3–PF4 showed no significant advantage from transitioning to a shared DC storage configuration. In this case, there is no reason to move from the simpler layout.

Table 4 expresses these results in terms of efficiencies, using the definitions (18) and (19). As anticipated, in some cases the efficiencies can exceed 100%.

Table 4. Achieved efficiencies of PF pairs, assessed by the two different proposed definitions.

	1 MW		2 MW		3 MW	
	η_{DC}	$\eta_{sharing}$	η_{DC}	$\eta_{sharing}$	η_{DC}	$\eta_{sharing}$
PF1–PF2	55%	42%	97%	65%	109%	64%
PF3–PF4	32%	0%	35%	0%	49%	0%
PF5–PF6	81%	61%	102%	66%	122%	68%

9.2. Results in Terms of Layout and Dimensions

Independently of the numerical values of the electrical parameters, it is important to evaluate a possible layout and dimension for the actual SC bank. To this aim, the SC module CapTop CTM 00165C0 0054V0 NN00 (shown in Figure 15), rated 54 V, 165 F, with a peak (limited to short times) current up to 2000 A, was used as a reference for the basic unit. Other manufacturers provide similar footprints and performances. This module was used to build standard cabinets having physical dimensions of $600 \times 1200 \times 2000$ (height) mm. So, the SC bank can be measured in terms of standard cabinets.

Figure 15. SC module CapTop CTM 00165C0 0054V0 NN00, rated 54 V and 165 F.

Table 5 presents the same concepts of Table 3 in terms of layout and dimensions, considering the reference SCs modules and cabinets.

Table 5. Comparison between the size, expressed in terms of number of reference cabinets and $N_s \times N_p$, of SC banks in the case of shared and independent DC storage.

	1 MW		2 MW		3 MW	
	Independent DC Links	Shared DC Links	Independent DC Links	Shared DC Links	Independent DC Links	Shared DC Links
PF1	14 cabinets (1×14)	24 cabinets (2×12)	12 cabinets (1×12)	14 cabinets (2×7)	9 cabinets (1×9)	12 cabinets (2×6)
PF2	28 cabinets (2×14)		28 cabinets (2×14)		24 cabinets (2×12)	
PF3	22 cabinets (2×11)	48 cabinets (2×24)	20 cabinets (2×10)	44 cabinets (2×22)	14 cabinets (2×7)	32 cabinets (2×16)
PF4	26 cabinets (2×13)		22 cabinets (2×11)		18 cabinets (2×9)	
PF5	44 cabinets (2×22)	32 cabinets (2×16)	44 cabinets (2×22)	24 cabinets (2×12)	40 cabinets (2×20)	20 cabinets (2×10)
PF6	32 cabinets (1×32)		25 cabinets (1×25)		22 cabinets (1×22)	

9.3. Optimization of Input Power

Another relevant aspect of the study was the analysis of the effect of the peak power absorption from the grid, which is useful for the design of the input charger and distribution grid. The results highlighted the following:

- Increasing the peak power limit from 1 MW to 2 MW resulted in a substantial reduction in the required energy for DC storage. Considering the reference SC modules and cabinets, this increase could save 18 reference cabinets.
- In comparison, the increase from 2 MW to 3 MW has less impact, for instance, only six reference cabinets.

This suggests that a peak power limit of 2 MW offers the best compromise between efficiency and practical feasibility. Details can be found in Tables 3 and 5.

Moreover, the average power drawn from the grid does not coincide with the fixed limit. For example, Figure 16 shows the instantaneous power drawn by the PS pair PF1–PF2 with P_{gridmax} = 2 MW per coil, clarifying that the assumed peak power is not constantly required, resulting in an average power around 2.2 MW (half of the allowed peak value). This could lead to further optimization in the distribution of the tokamak loads.
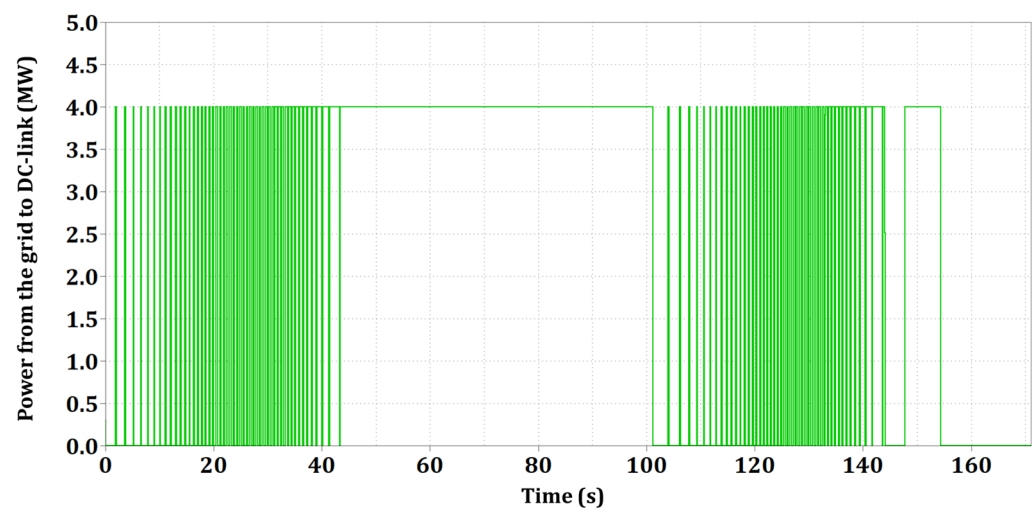

Figure 16. Instantaneous power drawn from the grid by the pair PF1–PF2.

As a result, the DC storage of the whole DTT PF PS system could consist of 14 + 42 + 24 = 80 cabinets occupying about 58 m^2 with an input power in the order of 10 MW (6 coils with a 2 MW peak). Alternatively, it could consist of 12 + 32 + 20 = 64 cabinets occupying about 46 m^2 with an input power in the order of 15 MW (3 MW peak). These results are rather impressive, considering that the installed power can exceed 500 MW.

10. Conclusions

This paper analyzed the design and optimization of a PS system for the PF coils of a tokamak. Even though the examples are focused on the last-generation tokamak DTT, the approach is generally applicable to all tokamaks and to other nuclear fusion plants.

The problem was approached both by theoretical formulations and by circuital simulations. This was possible after introducing the right foundations. The main steps for it were developed for the first time in this paper:

1. Defining a voltage and current reference scenario, including all the plasma phases.
2. Identifying analytical formulas and parameters to set and evaluate the optimization.
3. Designing a circuital model to include in its simulations all the tokamak phenomena.

The developed models and algorithms, also implemented in the PLECS software, will be available for future studies that may incorporate more detailed component behaviors and transient analyses. In particular, they are going to be implemented in a hardware-in-

the-loop (HIL) setup [44] combining the SC and H-bridge models with a real control board operating on the desired scenario.

The benefits of DC storage based on SC technology were extensively shown. Once these benefits were clarified, the design moved to the problem of identifying the best compromise between the size of SC banks and the power demand from the grid. The concept of complementary among the power and energy profiles of different PF coils was introduced for the first time and was crucial for the optimization. By leveraging the complementarity of shared DC storage, the peaks of power from the grid are limited both by temporal shifts (compensation of demand fluctuations over time) and by load balancing (distribution of energy storage requirements across multiple PSs). Such a rational use of available energy reduces the footprint of the DC storage, together with capital and operational costs, without affecting the required performance or the reliability and stability standards.

A comprehensive simulation campaign revealed that sharing the DC storage bank for the coil pairs PF1–PF2 and PF5–PF6 offers substantial benefits. For PF1–PF2, the shared storage configuration could potentially halve the required storage bank size, while for PF5–PF6, the reduction could be as significant as two-thirds.

At the same time, the analysis of the power demand from the grid demonstrated that increasing the peak power limit from 1 MW to 2 MW results in a more substantial reduction in the required energy for DC storage compared with the increase from 2 MW to 3 MW. This suggests that a peak power limit of 2 MW strikes the best balance between dimensions and efficiency. Considering the reference SC modules and cabinets, this corresponds to a saving of 18 cabinets for the PF system. The entire DC storage could consist of 80 or 64 cabinets occupying 58 m^2 or 46 m^2, respectively.

Observing the trend and the roadmap of SC technology independently of nuclear fusion applications, it is reasonable to predict that the dimensions and the costs of storage will decrease in the future. A more rapid improvement is expected for batteries due to the massive investments and the gigafactories under construction. Superconducting magnetic energy storage (SMES) is another technology that may be particularly suitable in fusion applications [6], with optimization problems similar to SC banks.

While the paper's results provide a clear direction for optimizing the DC storage and PS system, several practical considerations must be addressed for real-world implementation. Future works should focus on detailed implementation plans, including validation tests. In addition, they should assess alternative topologies (such as boost converters or hybrid storage joining SCs and batteries) that are able to overcome some intrinsic limitations noticed in this paper.

A relevant issue consists of the layout of the DC link for its connections to different PSs. This could introduce parasitic resistive and inductive effects that can detrimentally counterbalance the advantages of pairing the DC links. However, it is important to stress that both the PSs in a pair can be split into parallel units that can be connected to smaller DC links.

Another practical aspect to be considered is the selection of the technology, such as IGBTs or IGCTs, and the topology to be used, such as H-bridges or neutral point clamped (NPC). The simulations in this paper were based on a single H-bridge converter, as the primary focus was on the DC storage rather than on the converter control, while using H-bridges in parallel might be necessary to handle higher power levels and provide redundancy. In these situations, interphase inductors play a crucial role in ensuring proper operations and balancing currents between parallel H-bridges and in preventing circulating currents that could otherwise lead to inefficiencies and potential damage [56].

Safety is also an important aspect. The large energy stored in the coils must be carefully managed. A braking system (chopper) must always operate in parallel to the SC banks to avoid overvoltages/overcharges. A clear detection of full discharge is required for maintenance and settings (that are frequent in fusion experiments). It is interesting to note

that LICs can offer advantages in terms of specific energy, but they are more critical from the safety point of view.

Nevertheless, this paper presented some viable strategies for the solution of a very critical issue, almost a showstopper, for the exploitation of tokamaks as energy sources. In fact, the total power demand for the whole PF system was on the order of 10 MW. Such an optimized power exchange can reduce other power quality problems affecting the tokamaks, such as reactive power, harmonics, flicker, and oscillations.

Finally, it is important to stress that the analysis presented in this paper was applied to scenarios that were conceived by plasma physicists independently of any optimization of the electrical power or energy and without considering the option of (shared) DC storage. Therefore, the results could be even more significant in the future with an integrated approach that starts to consider possible power and energy optimization as a requirement from the beginning.

Also based on the guidelines and results of this paper, a Call for Tender for the realization of the DTT PF PS system is expected to be launched in 2025.

References

1. EUROfusion. European Research Roadmap to the Realisation of Fusion Energy. 2018. Available online: http://www.euro-fusion.org/eurofusion/roadmap/ (accessed on 20 August 2024).
2. ITER Website. Available online: http://www.iter.org (accessed on 20 August 2024).
3. Fusion Industry Association. Available online: https://www.fusionindustryassociation.org/ (accessed on 20 August 2024).
4. Wesson, J. *Tokamaks*, 3rd ed.; Clarendon Press: Oxford, UK, 2003.
5. Mitchell, N.; Zheng, J.; Vorpahl, C.; Corato, V.; Sanabria, C.; Segal, M.; Sorbom, B.N.; Slade, R.A.; Brittles, G.; Bateman, R.; et al. Superconductors for fusion: A roadmap. *Supercond. Sci. Technol.* **2021**, *34*, 103001. [CrossRef]
6. Gaio, E.; Ferro, A.; Lampasi, A.; Maistrello, A.; Dan, M.; Falvo, M.C.; Gasparini, F.; Lunardon, F.; Magnanimo, A.; Manganelli, M.; et al. Status and challenges for the concept design development of the EU DEMO Plant Electrical System. *Fusion Eng. Des.* **2022**, *177*, 113052. [CrossRef]
7. Ferro, A.; Lunardon, F.; Ciattaglia, S.; Gaio, E. The reactive power demand in DEMO: Estimations and study of mitigation via a novel design approach for base converters. *Fusion Eng. Des.* **2019**, *146*, 2687–2691. [CrossRef]
8. Tao, J.; Benfatto, I.; Goff, J.; Mankani, A.; Milani, F.; Song, I.; Tan, H.; Thomsen, J. ITER coil power supply and distribution system. In Proceedings of the 2011 IEEE/NPSS 24th Symposium on Fusion Engineering, Chicago, IL, USA, 26–30 June 2011; pp. 1–8.
9. Ferro, A.; Franke, T.; Gaio, E.; Bifaretti, S.; Bignucolo, F.; Biondi, R.; Rodriguez, P.B.; Caldora, M.; Chen, Z.; Dan, M.; et al. Overview on the applicability of the ITER/NPP-like technologies to the DEMO plant electrical system and promising alternatives. *IEEE Trans. Plasma Sci.* **2024**, 1–8. [CrossRef]

10. Minnucci, S.; Panella, S.; Ciattaglia, S.; Falvo, M.C.; Lampasi, A. Electrical Loads and Power Systems for the DEMO Nuclear Fusion Project. *Energies* **2020**, *13*, 2269. [CrossRef]

11. Barucca, L.; Bubelis, E.; Ciattaglia, S.; D'Alessandro, A.; Del Nevo, A.; Giannetti, F.; Hering, W.; Lorusso, P.; Martelli, E.; Moscato, I.; et al. Pre-conceptual design of EU DEMO balance of plant systems: Objectives and challenges. *Fusion Eng. Des.* **2021**, *169*, 112504. [CrossRef]

12. Ciattaglia, S.; Falvo, M.; Lampasi, A.; Proietti Cosimi, M. Energy Analysis for the Connection of the Nuclear Reactor DEMO to the European Electrical Grid. *Energies* **2020**, *13*, 2157. [CrossRef]

13. Di Pietrantonio, M.; Russo, G.; Guerra, E.; Minucci, S.; Lampasi, A.; Trotta, A.; Parisi, M.; Morandi, A. Design and Performance of a Linear Flux Pump for the Frascati Coil Cold Test Facility. *IEEE Trans. Appl. Supercond.* **2024**, *34*, 1–7. [CrossRef]

14. Magnanimo, A.; Teschke, M.; Griepentrog, G. Supercapacitors-based power supply for ASDEX upgrade toroidal field coils. *Fusion Eng. Des.* **2021**, *171*, 112574. [CrossRef]

15. Lampasi, A.; Pipolo, S.; Albanese, R.; Ambrosino, R.; Bifaretti, S.; Bojoi, R.; Bonaiuto, V.; Castaldo, A.; Caldora, M.; Cocchi, A.; et al. Overview of the Divertor Tokamak Test (DTT) coil power supplies. *Fusion Eng. Des.* **2023**, *188*, 113442. [CrossRef]

16. Gryaznevich, M.; Asunta, O.; Tokamak Energy Ltd. Team. Overview and status of construction of ST40. *Fusion Eng. Des.* **2017**, *123*, 177–180. [CrossRef]

17. Lampasi, A.; Tenconi, S.; Taddia, G.; Gherdovich, F.; Rinaldi, L. A new generation of power supplies for pulsed loads. *Fusion Eng. Des.* **2019**, *146*, 1921–1925. [CrossRef]

18. Nielsen, S.K.; Gryaznevich, M.P.; Jacobsen, A.S.; Jensen, T.; Jessen, M.; Korsholm, S.B.; Rasmussen, J.; Salewski, M.; Senstius, M.G.; Naulin, V.; et al. First results from the NORTH tokamak. *Fusion Eng. Des.* **2021**, *166*, 112288. [CrossRef]

19. Terlizzi, C.; Cocchi, A.; Lampasi, A.; Bifaretti, S. Design of Supercapacitor Bank and Filter to Mitigate Converter Interaction in a Tokamak Power Supply. In Proceedings of the 2021 IEEE International Conference on Environment and Electrical Engineering and 2021 IEEE Industrial and Commercial Power Systems Europe, Bari, Italy, 7–10 September 2021. [CrossRef]

20. Agredano-Torres, M.; Garcia-Sanchez, J.L.; Mancini, A.; Doyle, S.J.; Garcia-Munoz, M.; Ayllon-Guerola, J.; Barragán-Villarejo, M.; Viezzer, E.; Segado-Fernandez, J.; Lopez-Aires, D.; et al. Coils and power supplies design for the SMART tokamak. *Fusion Eng. Des.* **2021**, *168*, 112683. [CrossRef]

21. Onchi, T.; Idei, H.; Yanagi, N.; Zhang, Y.; Nakamura, K.; Kuroda, K.; Hasegawa, M.; Ikezoe, R.; Hanada, K.; Ido, T.; et al. Circuit design for doubling the toroidal magnetic field on the QUEST spherical tokamak. *Fusion Eng. Des.* **2023**, *192*, 113794. [CrossRef]

22. Song, Z.; Tan, Y.; Wang, S.; Wang, B.; Chang, T.; Chen, R. A hybrid cascaded H-bridge converter for poloidal magnets of tokamaks. *IEEE Trans. Plasma Sci.* **2024**, 1–6. [CrossRef]

23. Martone, R.; Albanese, R.; Crisanti, F.; Martin, P.; Pizzuto, A. *DTT Divertor Tokamak Test Facility–Interim Design Report*; ENEA Italian National Agency for New Technologies: Rome, Italy, 2019.

24. Crisanti, F.; Giruzzi, G.; Martin, P. *Divertor Tokamak Test Facility Research Plan Version 1.0.*, 1st ed.; ENEA: Rome, Italy, 2024.

25. Romanelli, F. Divertor Tokamak Test facility Project: Status of Design and Implementation. *Nucl. Fusion* **2024**, *64*, 112015. [CrossRef]

26. Chiappa, A.; Groth, C.; Biancolini, M.E.; Bachmann, C.; Maviglia, F.; Tomarchio, V. Reshaping the DEMO Tokamak's TF Coil with High Fidelity Multiphysics CAE and Advanced Mesh Morphing. *Newsletter EnginSoft*, 2021; Year 18 n°3.

27. Castaldo, A.; Albanese, R.; Ambrosino, R.; Crisanti, F. Plasma Scenarios for the DTT Tokamak with Optimized Poloidal Field Coil Current Waveforms. *Energies* **2022**, *15*, 1702. [CrossRef]

28. Acampora, E.; Ambrosino, R.; Castaldo, A.; Iervolino, R. Magnetic control of DTT alternative plasma configurations. *Fusion Eng. Des.* **2023**, *192*, 113617. [CrossRef]

29. Casiraghi, I.; Mantica, P.; Ambrosino, R.; Aucone, L.; Baiocchi, B.; Balbinot, L.; Barberis, T.; Castaldo, A.; Cavedon, M.; Frassinetti, L.; et al. Core integrated simulations for the Divertor Tokamak Test facility scenarios towards consistent core-pedestal-SOL modelling. *Plasma Phys. Control. Fusion* **2023**, *65*, 035017. [CrossRef]

30. Lampasi, A. Benefits of high-energy varistors in breakdown and fast discharge units. *Fusion Eng. Des.* **2023**, *187*, 113366. [CrossRef]

31. Caldora, M.; Falvo, M.C.; Lampasi, A.; Marelli, G. Preliminary design of the electrical power systems for DTT nuclear fusion plant. *Appl. Sci.* **2021**, *11*, 5446. [CrossRef]

32. Deven Updates. Available online: https://cfs.energy/devens-campus/updates (accessed on 19 March 2024).

33. Shimada, K.; Baulaigue, O.; Cara, P.; Coletti, A.; Coletti, R.; Matsukawa, M.; Terakado, T.; Yamauchi, K. Design study of an AC power supply system in JT-60SA. *Fusion Eng. Des.* **2011**, *86*, 1427–1431. [CrossRef]

34. Kar, K. *Handbook of Nanocomposite Supercapacitor Materials II: Performance*; Springer: Berlin, Germany, 2020. [CrossRef]

35. Choi, M.E.; Kim, S.W.; Seo, S.W. Energy Management Optimization in a Battery/Supercapacitor Hybrid Energy Storage System. *IEEE Trans. Smart Grid* **2012**, *3*, 463–472. [CrossRef]

36. Zhang, Q.; Li, G. Experimental study on a semi-active battery-supercapacitor hybrid energy storage system for electric vehicle application. *IEEE Trans. Power Electron.* **2019**, *35*, 1014–1021. [CrossRef]

37. Rafik, F.; Gualous, H.; Gallay, R.; Crausaz, A.; Berthon, A. Frequency, thermal and voltage supercapacitor characterisation and modelling. *J. Power Sources* **2007**, *165*, 928–934. [CrossRef]

38. Navarro, G.; Nájera, J.; Torres, J.; Blanco, M.; Santos, M.; Lafoz, M. Development and experimental validation of a supercapacitor frequency domain model for industrial energy applications considering dynamic behaviour at high frequencies. *Energies* **2020**, *13*, 1156. [CrossRef]

39. Musolino, V.; Piegari, L.; Tironi, E. New Full-Frequency-Range Supercapacitor Model with Easy Identification Procedure. *IEEE Trans. Ind. Electron.* **2013**, *60*, 112–120. [CrossRef]

40. Morandi, A.; Lampasi, A.; Cocchi, A.; Gherdovich, F.; Melaccio, U.; Ribani, P.L.; Rossi, C.; Soavi, F. Characterization and Model Parameters of Large Commercial Supercapacitor Cells. *IEEE Access* **2021**, *9*, 20376–20390. [CrossRef]

41. Christen, T.; Carlen, M.W. Theory of Ragone plots. *J. Power Sources* **2000**, *91*, 210–216. [CrossRef]

42. Reichbach, N.; Mellincovsky, M.; Peretz, M.M.; Kuperman, A. Long-Term Wide-Temperature Supercapacitor Ragone Plot Based on Manufacturer Datasheet. *IEEE Trans. Energy Convers.* **2016**, *31*, 404–406. [CrossRef]

43. Murray, D.B.; Hayes, J.G. Cycle Testing of Supercapacitors for Long-Life Robust Applications. *IEEE Trans. Power Electron.* **2015**, *30*, 2505–2516. [CrossRef]

44. Terlizzi, C.; Bifaretti, S.; Lampasi, A. Current Sharing Control Modeling and Design for Power Supplies in Nuclear Fusion Applications. *IEEE Trans. Ind. Appl.* **2024**, *60*, 3427–3437. [CrossRef]

45. Al Sakkaa, M.; Gualous, H.; Van Mierlo, J. Characterization of supercapacitors matrix. *Electrochem. Acta* **2010**, *55*, 7532–7537. [CrossRef]

46. Ye, Y.; Cheng, K.W.E. Modeling and Analysis of Series–Parallel Switched-Capacitor Voltage Equalizer for Battery/Supercapacitor Strings. *IEEE J. Emerg. Sel. Top. Power Electron.* **2015**, *3*, 4. [CrossRef]

47. Yassine, M.; Fabris, D. Performance of Commercially Available Supercapacitors. *Energies* **2017**, *10*, 1340. [CrossRef]

48. Kuperman, A.; Mellincovsky, M.; Lerman, C.; Aharon, I.; Reichbach, N.; Geula, G.; Nakash, R. Supercapacitor Sizing Based on Desired Power and Energy Performance. *IEEE Trans. Power Electron.* **2013**, *29*, 5399–5405. [CrossRef]

49. Zubieta, L.B.; Bonert, R. Characterisation of double-layer capacitors for power electronics applications. *IEEE Trans. Ind. Appl.* **2000**, *36*, 199–205. [CrossRef]

50. Cocchi, A.; Lampasi, A. Modeling Non-Ideal Behaviors of Supercapacitors' Equivalent Capacitance. In Proceedings of the 20th IEEE International Conference on Environment and Electrical Engineering (EEEIC 2020), Madrid, Spain, 9–12 June 2020.

51. Navarro, G.; Blanco, M.; Torres, J.; Nájera, J.; Santiago, Á.; Santos-Herran, M.; Ramírez, D.; Lafoz, M. Dimensioning Methodology of an Energy Storage System Based on Supercapacitors for Grid Code Compliance of a Wave Power Plant. *Energies* **2021**, *14*, 985. [CrossRef]

52. Nybeck, C.N.; Dodson, D.A.; Wetz, D.A.; Heinzel, J.M. Characterization of ultracapacitors for transient load applications. *IEEE Trans. Plasma Sci.* **2019**, *47*, 2493–2499. [CrossRef]

53. Marracci, M.; Tellini, B.; Catelani, M.; Ciani, L. Ultracapacitor Degradation State Diagnosis via Electrochemical Impedance Spectroscopy. *IEEE Trans. Instrum. Meas.* **2015**, *64*, 1916–1921. [CrossRef]

54. Manla, E.; Mandic, G.; Nasiri, A. Development of an Electrical Model for Lithium-Ion Ultracapacitors. *IEEE J. Emerg. Sel. Top. Power Electron.* **2015**, *3*, 395–404. [CrossRef]

55. *JT-60SA Plant Integration Document (PID)*, Version 4.4. 2023.

56. Wasiq, M.; Terlizzi, C.; Bifaretti, S.; Lampasi, A. Design of High-Current Converters with Inter-cell Transformer. In Proceedings of the 2023 IEEE Energy Conversion Congress and Exposition (ECCE), Nashville, TN, USA, 29 October–2 November 2023; IEEE: New York, NY, USA, 2023; pp. 5819–5826.